JACS
JOURNAL OF THE AMERICAN CHEMICAL SOCIETY
Article
pubs.acs.org/JACS

Hemilabile Bridging Thiolates as Proton Shuttles in Bioinspired H_2 Production Electrocatalysts

Shengda Ding,[†,§] Pokhraj Ghosh,[†,§] Allen M. Lunsford,[†,§] Ning Wang,[†,‡] Nattamai Bhuvanesh,[†] Michael B. Hall,[*,†] and Marcetta Y. Darensbourg[*,†]

[†]Department of Chemistry, Texas A & M University, College Station, Texas 77843, United States

Supporting Information

ABSTRACT: Synthetic analogues and computationally assisted structure−function analyses have been used to explore the features that control proton−electron and proton−hydride coupling in electrocatalysts inspired by the [NiFe]-hydrogenase active site. Of the bimetallic complexes derived from aggregation of the dithiolato complexes MN_2S_2 (N_2S_2 = bismercaptoethane diazacycloheptane; M = Ni or Fe(NO)) with $(\eta^5\text{-}C_5H_5)Fe(CO)^+$ (the **Fe′** component) or $(\eta^5\text{-}C_5H_5)Fe(CO)_2^+$, **Fe″**, which yielded **Ni−Fe′**$^+$, **Fe−Fe′**$^+$, **Ni−Fe″**$^+$, and **Fe−Fe″**$^+$, respectively, both **Ni−Fe′**$^+$ and **Fe−Fe′**$^+$ were determined to be active electrocatalysts for H_2 production in the presence of trifluoroacetic acid. Correlations of electrochemical potentials and H_2 generation are consistent with calculated parameters in a predicted mechanism that delineates the order of addition of electrons and protons, the role of the redox-active, noninnocent NO ligand in electron uptake, the necessity for Fe′−S bond breaking (or the hemilability of the metallodithiolate ligand), and hydride-proton coupling routes. Although the redox active $\{Fe(NO)\}^7$ moiety can accept and store an electron and subsequently a proton (forming the relatively unstable Fe-bound HNO), it cannot form a hydride as the NO shields the Fe from protonation. Successful coupling occurs from a hydride on **Fe′** with a proton on thiolate S and requires a propitious orientation of the H−S bond that places H^+ and H^- within coupling distance. This orientation and coupling barrier are redox-level dependent. While the **Ni−Fe′** derivative has vacant sites on both metals for hydride formation, the uptake of the required electron is more energy intensive than that in **Fe−Fe′** featuring the noninnocent NO ligand. The Fe′−S bond cleavage facilitated by the hemilability of thiolate to produce a terminal thiolate as a proton shuttle is a key feature in both mechanisms. The analogous Fe″−S bond cleavage on **Ni−Fe″** leads to degradation.

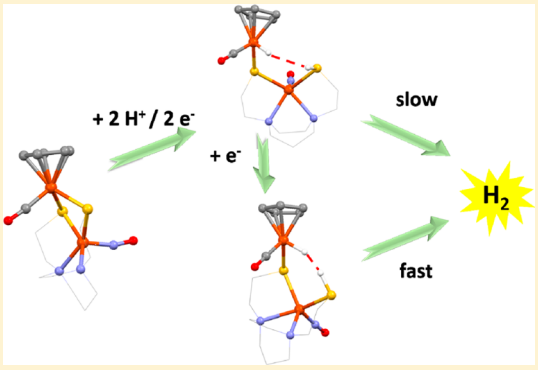

INTRODUCTION

Heterobimetallic molecular compositions utilizing thiolate-sulfurs as bridges are widespread in biology, especially in the active sites of metalloenzymes such as the [FeFe]- and [NiFe]-H_2ase and acetyl CoA synthase.[1,2] That these biocatalysts facilitate organometallic-like transformations, using first-row/abundant transition metals, has inspired chemists to address the features that control their mechanisms of action through the synthetic-analogue approach. Synergy between synthesis and theory has developed by linking the mechanistic interpretation of assays, such as electrocatalytic proton reduction or hydrogen oxidation in the active sites of the hydrogenases, with those of the model complexes.[3] While the structures of individual components of the biocatalysts that are site-isolated by the protein are clear, functional reproductions in small molecule models have not been entirely successful. The role of a pendant amine base nearby an open site on iron was determined to be critical to the remarkable rates of hydrogen production in the [FeFe]-H_2ase[2] and has been successfully used to design H^+ reduction and H_2 oxidation electrocatalysts in nickel-based complexes outfitted with the PNP- and P_2N_2-type ligands of Dubois et al.[3−8] Their team has also provided dramatic, *bona fide* examples of heterolytic H_2 cleavage products in $(\eta^5\text{-}C_5H_4R)Fe^{II}(P_2N_2)^+$ complexes, suggesting that the P_2N_2 ligand in structure I, and its pendant base capabilities, might be considered as a surrogate for the $Ni(SR)_4$ metalloligand in the [NiFe]-H_2ase active site.[9−11] Thus, while the catalytic center of [NiFe]-H_2ase does not have a pendant amine as operative base, there is structural support from high-resolution protein crystallography that a terminal cysteinyl thiolate on the nickel might serve in that capacity.[12,13] Such a suggestion was made earlier in the mechanistic study of Niu and Hall.[14] Other persistent questions regarding the requirement of two metals in such active sites are as follows: Do they assist each other by dual electron storage? Does one tune the electronic character and redox potential of the other? Is a metallodithiolate biology's ultimate redox-active, noninnocent ligand?

There is an extensive class of bi- and polymetallic complexes derived from transition metals, largely Ni^{II}, in tetradentate $E_2S_2^{2-}$ (E = N, P, S) binding sites that use excess lone pairs on the cis thiolate sulfurs for binding in a bidentate manner to an

Received: June 30, 2016
Published: August 19, 2016

DOI: 10.1021/jacs.6b06461
J. Am. Chem. Soc. 2016, 138, 12920−12927

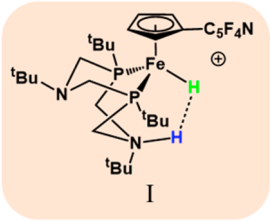

I

additional metal, M′.[15,16] Analogous to the (η^5-C_5H_4R)-$Fe^{II}(P_2N_2)^+$ complexes described above, myriad heterobimetallics have been reported in a developing area that uses η^5-cyclopentadienide (η^5-C_5H_5 or η^5-C_5Me_5, i.e., Cp and Cp*, respectively) or η^6-arenes bound to d^6 Fe^{II} or Ru^{II}, as M′, which in combination with the bridging dithiolates from the NiN_2S_2 may offer a single open site for reactivity at M′, structure II.[15,17−22] The tunability at the π-ligand offers some control for oxidative addition in stoichiometric reactions, including both H_2 and O_2 activation.[23−26] Reports of proton reduction under electrochemical conditions by such $CpFe^{II}$ or $CpRu^{II}$ entities are scarce in the literature; however, there are examples of an S'_2NiS_2 (S′ = thioether sulfur; S = thiolate sulfur) metalloligand bound to CpFe′ and Cp*Fe′ that demonstrated modest electrocatalysis and H_2 production.[18,20] The MN_2S_2 platform offers opportunity to modify a metallodithiolate ligand by changing only the M, retaining consistency in steric features such that the S-donor and M′-acceptor effects might be deconvoluted. Thus, we have designed experimental and computational protocols to analyze the proton reduction possibilities of the heterobimetallics represented in Scheme 2. The focus is on the potential sites for electron and proton uptake, the order of their addition, and the requirements for hemilability and S-protonation of the MN_2S_2 metallodithiolate ligands at various redox levels.

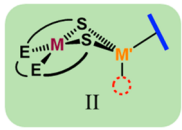

II

RESULTS

Synthesis and Characterization. Scheme 1 displays the synthetic protocol used to prepare the bimetallic complexes, MN_2S_2·CpFe(CO)$^+BF_4^-$ (M = Fe(NO), Ni; the Fe in CpFe(CO) is Fe′ in this work), **Fe−Fe′**$^+$ and **Ni−Fe′**$^+$. The reaction of MN_2S_2 and [$CpFe(CO)_2$(Solv)]$^+$, prepared *in situ* from $CpFe(CO)_2I$ and $AgBF_4$ in CH_2Cl_2, at 22 °C, formed intermediate species MN_2S_2·$CpFe(CO)_2^+BF_4^-$, **Fe−Fe″**$^+$ and **Ni−Fe″**$^+$ (the Fe in $CpFe(CO)_2$ is Fe″). Subsequent photolysis released CO and permitted bidentate binding of the metallodithiolate ligands. While the intermediate species, **Fe−Fe″**$^+$ and **Ni−Fe″**$^+$, are light and air sensitive, the **Fe−Fe′**$^+$ and **Ni−Fe′**$^+$ complexes are isolated as intensely colored crystalline BF_4^- salts that are thermally and air stable in the solid form. Stringent conditions (CO pressure of 11 bar and 50 °C) partially return the MFe′$^+$ to the MFe″$^+$, see Figure S9.

X-ray diffraction analysis of crystalline **Ni−Fe′**$^+$, **Fe−Fe′**$^+$, and **Ni−Fe″**$^+$ revealed molecular structures with typical piano-stool geometry about the $CpFe'(CO)^+$ unit and butterfly-like [M(μ-SR)$_2$Fe′] cores in the **Ni−Fe′**$^+$ and **Fe−Fe′**$^+$ derivatives, Scheme 2. Specifically, the bridging thiolate sulfur lone pairs impose a hinge angle (the intersection of the best N_2S_2 plane with the S_2Fe' plane) of ca. 125°. The mesocyclic

Scheme 1. Synthesis of Fe−Fe′$^+$ **and Ni−Fe′**$^+$ **Complexes as BF_4^- Salts**[a]

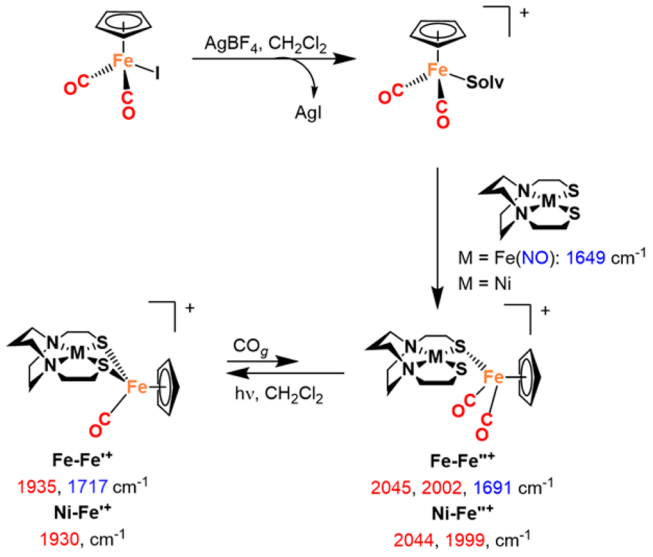

[a]The IR frequencies of CO and NO are in red and blue, respectively.

Scheme 2. Molecular Structures of Ni−Fe″$^+$**, Fe−Fe′**$^+$**, and Ni−Fe′**$^+$ **Complexes with the BF_4^- Ions Omitted for Clarity**

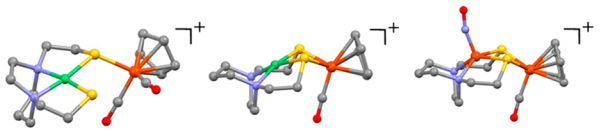

	Ni-Fe″+	Ni-Fe′+	Fe-Fe′+
M• • •Fe/Å	3.887 (2)	3.016 (1)	3.209 (1)
∠M-N-O/°	---	---	163.8 (3)
M-S/Å	2.172 (3)[a], 2.149 (3)[b]	2.152 (3)[c]	2.235 (1)[c]
Fe-S/Å	2.285 (3)[a], 3.999 (3)[b]	2.291 (3)[c]	2.285 (1)[c]
Hinge Angle/°	---	126.23	124.85

[a]Bonded sulfur. [b]Nonbonded sulfur [c]Average M−S distance

diazacycloheptane framework in the MN_2S_2 portion of each provides similar N···N and S···S distances, and $\angle_{S-Fe'-S}$ of ca. 82°. In the **Fe−Fe′**$^+$ complex the NO is transoid to the CO on the CpFe′ unit; the $\angle_{Fe-N-O}$ angle is 163.8°. The M···Fe′ distances in **Fe−Fe′**$^+$ and **Ni−Fe′**$^+$ are 3.203(1) and 3.016(1) Å, respectively. In contrast, the **Ni−Fe″**$^+$ dicarbonyl complex finds the NiN_2S_2 plane is shifted away from where it was in the **Ni−Fe′**$^+$, opening the Ni−S−Fe″ bond angle to ca. 121.4(1)° from ca. 85.44(3)° in the **Ni−Fe′**$^+$ and yielding a Ni−Fe" distance some 0.7 to 0.9 Å greater than in the bidentate MN_2S_2−Fe′ complex. The Fe″−S dative bond distance in **Ni−Fe″**$^+$ is 2.285(3) Å, and the nonbonded thiolate S is at 3.999(3)Å from the Fe".

While the **Ni−Fe′**$^+$ complex is diamagnetic, the **Fe−Fe′**$^+$ has $S = 1/2$, consistent with the well-known {Fe(NO)}^{7} electronic configuration.[27,28] The 298 K, X-band EPR spectrum shows an isotropic triplet of g value = 2.04 with hyperfine coupling constant of 15.3 G, and only minor differences to the free metalloligand.[29] Details of the low- and variable-field Mössbauer spectra of the **M−Fe′**$^+$ and **M−Fe″**$^+$ complexes will be presented and discussed in a separate study.

Electrochemistry. Cyclic voltammograms (CV) of BF_4^- salts of **Fe−Fe′**$^+$, Figure S30, and **Ni−Fe′**$^+$, Figure S34, were recorded at 22 °C under Ar. All scans are referenced to internal $Fc^{0/+}$ at $E_{1/2}$ = 0.0 V. Full scans of both complexes initiated in the positive direction as well as peak isolation and scan rate

DOI: 10.1021/jacs.6b06461
J. Am. Chem. Soc. 2016, 138, 12920−12927

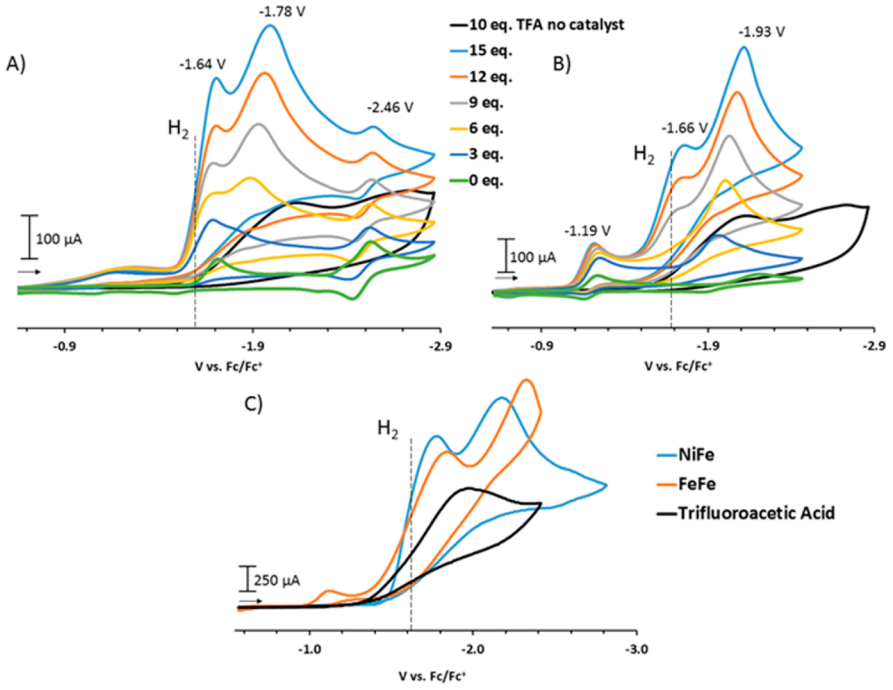

Figure 1. CV of 2 mM (A) **Ni−Fe′**$^{+}$ and (B) **Fe−Fe′**$^{+}$ under Ar in CH_3CN solutions containing 0.1 M [$^{t}Bu_4N$][PF_6] as supporting electrolyte with addition of equivalents of TFA. (C) An overlay of **Ni−Fe′**$^{+}$ and **Fe−Fe′**$^{+}$ in the presence of 50 equiv of TFA as well as 50 equiv of TFA in the absence of either catalyst. The dotted line denotes the potential applied during bulk electrolysis, −1.56 V.

dependence can be found in Figures S30−S37. On initiating the electrochemical scan in the cathodic direction, two reduction events and, upon reversal, two oxidation events were observed for both complexes within the MeCN solvent window. The initial reductive event, at −1.64 V in the case of the **Ni−Fe′**$^{+}$, is assigned to the $Ni^{II/I}$ couple; its irreversibility is addressed in the computational section below. In contrast, for the **Fe−Fe′**$^{+}$ complex, the first reduction is quasi-reversible and at a more positive position, −1.19 V; it is assigned to the {Fe(NO)}$^{7/8}$ redox couple. In both cases, the first observed or more positive reduction event is anodically shifted compared to the MN_2S_2 (free metalloligand) precursors, thus illustrating the electron-withdrawing nature of the [CpFe′(CO)]$^{+}$ unit and its ability to modulate redox events on the MN_2S_2 unit.[28,30] The second, more negative, irreversible reduction event in the **Fe−Fe′**$^{+}$ complex is assigned to the $Fe'^{II/I}$ couple in the [CpFe′(CO)]$^{+}$ unit. For the **Ni−Fe′**$^{+}$ complex, assignment of the more negative event is not straightforward due to the irreversibility of the previous redox event; computational studies, *vide infra*, indicate an intramolecular Ni^{I} to Fe^{II} electron transfer concomitant with structural rearrangement accounts for this irreversible behavior.

Addition of trifluoroacetic acid (TFA) to the electrochemical cell containing **Ni−Fe′**$^{+}$ or **Fe−Fe′**$^{+}$ increases the current of the initial reduction events described above. (Methanesulfonic acid gave similar results as TFA, see Figure S38−S39, however considerable fouling of the electrode surface discouraged extensive studies with this acid.) For the **Ni−Fe′**$^{+}$ complex, this current continues to increase with additional equivalents of TFA, Figure 1A, while for the **Fe−Fe′**$^{+}$ complex the initial reduction event's current is saturated after addition of 12 equiv of TFA, Figure 1B. With >6 equiv of TFA, a new peak at −1.66 V appears for the **Fe−Fe′**$^{+}$ complex, and its intensity increases with additional equiv of TFA. An overlay of both complexes after addition of 50 equiv of TFA as well as TFA in the absence of either catalyst is displayed in Figure 1C. The large current enhancement was attributed to the catalytic production of H_2, which was quantified by bulk electrolysis studies described below. From the CV experiments, turnover frequencies (TOFs) of 69 and 52 s^{-1} (experimental barriers: 14.9 and 15.1 kcal/mol at 298.15 K by Eyring equation) and overpotentials of 938 and 942 mV for the **Fe−Fe′**$^{+}$ and **Ni−Fe′**$^{+}$ complexes, respectively, were obtained.[31−33] The calculation of TOFs and overpotentials follows the approach described by Helm, Appel, and Wiese, see the SI for specifics.[33,34] It is noteworthy to mention the observed barrier is a comprehensive parameter reflecting the activation of electron transfer, proton transfer, and intra/intermolecular processes throughout the catalytic cycle. It is often higher than the calculated barriers of intramolecular processes, *vide infra*. The H/D kinetic isotope effects on **Fe−Fe′**$^{+}$ and **Ni−Fe′**$^{+}$ turnover frequencies (k_H/k_D) were determined to be 1.46 and 1.56, respectively. While k_H/k_D isotope effects are known to vary widely, these relatively low ratios are consistent with the likely involvement of metal-hydride species in the catalytic cycles.[35,36]

Electrocatalytic H_2 Production. The headspace of the bulk electrolysis setup was analyzed for H_2 using gas chromatography after applying a constant potential at −1.56 V (dotted line in Figure 1) in the presence of catalyst and 50 equiv of TFA. Due to the overlap of the background TFA peak and the catalytic peaks, the H_2 evolving from the acid itself must be deducted, Table S3. All values obtained are an average of three separate bulk electrolysis experiments. After 30 min of electrolysis with the **Ni−Fe′**$^{+}$ catalyst, 0.98 ± 0.04 Coulombs (after acid subtraction) was passed through the solution resulting in a turnover number (TON) of 0.26 ± 0.01 with a Faradaic efficiency of 96.0 ± 2.9% for H_2 production, Table S4. Similarly in the presence of the **Fe−Fe′**$^{+}$ catalyst, passage of 1.29 ± 0.06 Coulombs through the solution gave a TON of 0.33 ± 0.02 with a Faradaic efficiency of 77.2 ± 7.9% for H_2,

DOI: 10.1021/jacs.6b06461
J. Am. Chem. Soc. 2016, 138, 12920−12927

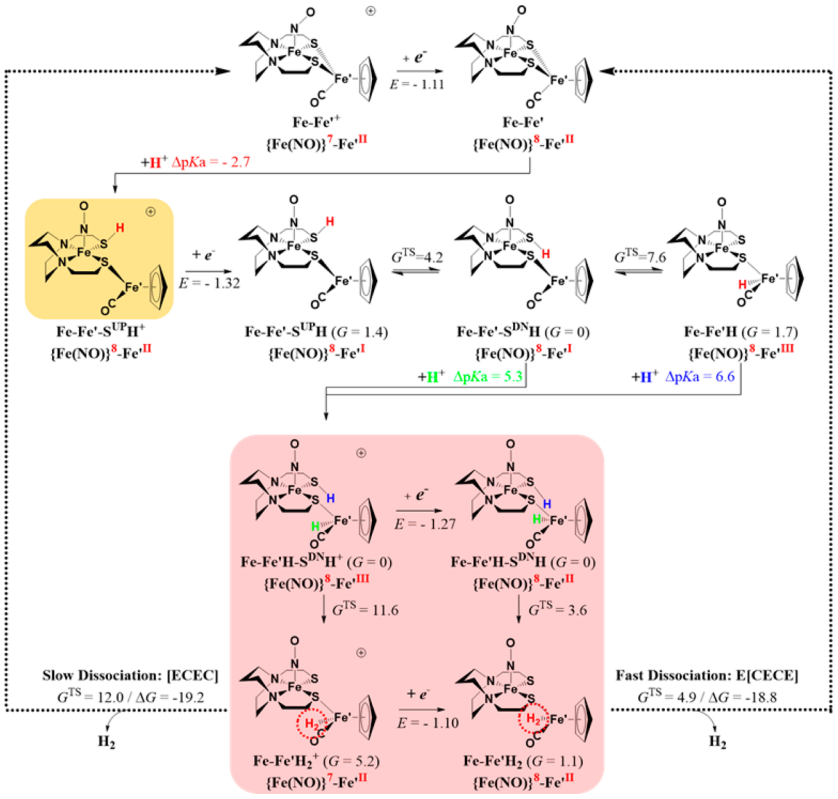

Figure 2. Calculated electrocatalytic cycles for H_2 production on **Fe−Fe′**$^{+}$ in the presence of TFA. The relative Gibbs free energies are provided in kcal/mol and the reference point (G = 0) resets after every reduction or protonation. The redox potentials (E) are reported in V with reference to the standard redox couple $Fc^{+/0}$ and the relative acidities (ΔpK_a) are reported with reference to TFA. Note: superscripts DN and UP on S refer to the positioning of the proton in S-protonated species.

Table S5. These results confirm that the current enhancement in the CV is in fact due to the reduction of protons to H_2 by the **Ni−Fe′**$^{+}$ and **Fe−Fe′**$^{+}$ catalysts in the presence of TFA.

Computational Investigation: Assignment of Redox Events and Mechanistic Studies. The complexities of the CVs of the **Ni−Fe′**$^{+}$ or **Fe−Fe′**$^{+}$ complexes in the presence of added acid, which indicate the existence of protonated and/or rearranged species, stimulated computational studies as complements to electrocatalytic proton reduction studies. A minimum of two chemical steps (C steps, i.e., protonation) and two electrochemical steps (E steps, i.e., reduction) is required to produce H_2 from protons and electrons. The exact order of C and E steps depends on the pK_a of the acid vs catalyst and the redox potential of the catalyst, respectively; they often take place in an alternating order to prevent the accumulation of charges.[37] To computationally construct the E and C steps in catalytic cycles, structures of the precursor complexes from X-ray diffraction were compared to the calculated structures as validity checks, Table S11; the redox potentials (E^0 vs $Fc^{+/0}$) and relative acidities ($\Delta pK_a = pK_a$ (CatH) $- pK_a(CF_3COOH)$) of components were predicted by calculations. Alternative sites for location of the added protons were carefully examined to determine which sites were lowest in energy. Detailed methodology information and optimized geometries (xyz files) are deposited in the SI.

Computational approaches to electrocatalytic proton reduction mechanisms have become fairly standard,[37−39] especially for biomimetics of the hydrogenase active sites. From protein crystallography, the features of the protein ensconced molecular catalysts and second coordination spheres are readily apparent but their roles are just beginning to be firmly established.[1] Hence, our starting points for the predicted mechanisms lie in paths deemed reasonable for the biocatalysts and for previous studies of biomimics; structures are accepted or rejected according to comparative energies (E^0 and pK_a) and activation barriers between structures. The bimetallic constitution of our complexes, **Fe−Fe′**$^{+}$ and **Ni−Fe′**$^{+}$, enables them to buffer electrons, with additional stabilization from the noninnocent ligands, particularly NO in the case of **Fe−Fe′**$^{+}$.[29] At some point, typically after reduction(s), a complex must be able to accept a proton, convert it into a hydride on the metal, be poised to react with an additional proton, located on some basic site, to yield H_2. Our model complexes, however, lack an obvious built-in pendant base to serve as a proton reservoir, a role played by the bridgehead amine in [FeFe]-H_2ase[1,38,40−42] or a terminal thiolate in the [NiFe]-H_2ase active site.[1,12,13] Instead, the hemilabile bridging thiolates on **Fe−Fe′**$^{+}$ and **Ni−Fe′**$^{+}$ may dissociate one of two Fe′−S bonds; the veracity of such a monodentate S-bridging species is supported by the isolated **Ni−Fe″**$^{+}$ shown in Scheme 1. Such dissociation creates reactive sites both on S and Fe′, i.e., a Lewis acid−base pair that can be used as proton and hydride storage depots is generated. Interestingly, the possibility of conversion of a bridging thiolate into an available proton base was inspired by the early theoretical studies of the [FeFe]-H_2ase.[38,43] The advent of semisynthetic approaches to biohybrids in recent years that unambiguously identified a bridgehead amine in the S to S linker of the diiron unit in [FeFe]-H_2ase has established the pivotal role of this pendant base in proton transfer, thus

DOI: 10.1021/jacs.6b06461
J. Am. Chem. Soc. 2016, 138, 12920−12927

negating the requirement for Fe−S bond cleavage in such functionalized dithiolates.[44−47]

Figures 2 and 3 display the calculated electrocatalytic cycles for H_2 production with **Fe−Fe′**$^{+}$ and **Ni−Fe′**$^{+}$, respectively, as

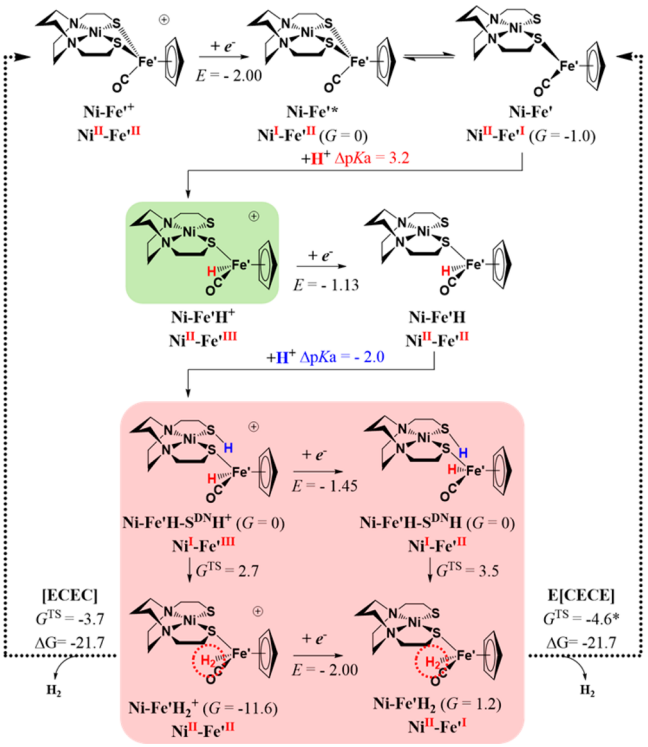

Figure 3. Calculated electrocatalytic cycles for H_2 production on **Ni−Fe′**$^{+}$ in the presence of TFA; see caption of Figure 2 for additional description. The Gibbs free energy of the barrier between **Ni−Fe′H$_2$** and **Ni−Fe′**, G = −4.6 kcal/mol, as marked with an asterisk, is lower than that of **Ni−Fe′H$_2$**, G = 1.2 kcal/mol. This is caused by the preference of solvation correction over the transition state. This transition may be accepted as barrierless.

electrocatalysts. A description of the former is as follows. In the absence of added acid, the CV scans of **Fe−Fe′**$^{+}$ show two reduction events; the first quasi-reversible one was calculated to be −1.11 V (exp. −1.19 V) and is assigned to the Fe(NO) unit, i.e., the redox couple {Fe(NO)}$^{7/8}$-Fe′^{II}. Such an assignment was confirmed by the IR shifts of the diatomic ligands (exp.: −57 and −23 cm^{-1}; calcd −84 and −31 for NO and CO, respectively, Figure S11, Table S12). The resulting neutral **Fe−Fe′** has a linear triplet {Fe(NO)}^{8} moiety, formed by high-spin Fe^{II} antiferromagnetically coupled to high-spin NO^{-}.[29,48] It may be further reduced irreversibly, calculated at −1.99 V (exp. −2.07 V), to **Fe−Fe′**$^{-}$, in which one S−Fe′ bond dissociates to accommodate the added electron on Fe′ with a final redox level of {Fe(NO)}^{8}-Fe′^{I}.

In the presence of TFA the first reduction event at −1.19 V in the CV was observed to increase in current without shifting position. This behavior is explained by the reaction of TFA with the reduced **Fe−Fe′** state and its depletion, thus enhancing diffusion of **Fe−Fe′**$^{+}$ into the double layer at the electrode. By calculations, the thiolate S was determined to be the optimal protonation site. Other possibilities (Table S9) were considered, including the iron-bound NO which would produce the HNO ligand. It was found however to be thermodynamically less likely and also nonproductive for subsequent H_2 formation as a metal-hydride is needed for the H^{+}/H^{-} coupling. Upon protonation on sulfur the bond cleavage at Fe′−S immediately follows, stabilizing the system by 3.7 kcal/mol. The ΔpK_a (vs TFA) values for ring-closed (**Fe−Fe′-S*H**$^{+}$) and ring-opened (**Fe−Fe′−S^{UP}H**$^{+}$) sulfur-protonated species are −5.6 and −2.7, respectively, indicating slightly unfavorable thermodynamic processes. Thus, excess acid is needed to drive the protonation of **Fe−Fe′**, explaining why the observed saturation of current enhancement requires multiple equivalents (>12 equiv) of added acid and rules out the possibility of an immediate second protonation on **Fe−Fe′−S^{UP}H**$^{+}$ (to **Fe−Fe′H−S^{DN}H**$^{2+}$, ΔpK_a = −14.3). Despite the increase in current response, the electrochemical event at −1.11 V (−1.19 V exp.) is not catalytic, as this reduction potential is insufficient (*vide infra*) to pass a second electron and close the catalytic cycle.

A second current enhancement, which appears in CV scans with added acid at −1.66 V (shifted by 0.41 V from −2.07 V in the absence of acid), suggests reactions of new species, **Fe−Fe′−S^{UP}H**$^{+}$, generated by protonation. One should be reminded that the production of **Fe−Fe′−S^{UP}H**$^{+}$ is energetically unfavorable such that the reduction event of **Fe−Fe′−S^{UP}H**$^{+}$ observed at −1.66 V becomes dominant only with the presence of more than 6 equiv of TFA. The reduction of **Fe−Fe′−S^{UP}H**$^{+}$ has a calculated potential of −1.32 V, changing the Fe^{II} of Fe′ to Fe^{I}, a redox state capable of converting a proton into a hydride. The direct product of reduction, **Fe−Fe′−S^{UP}H** (G = 1.4 kcal/mol) may transform into a hydride-bearing species **Fe−Fe′H** (G = 1.7 kcal/mol) via the S−H inversion species **Fe−Fe′−S^{DN}H** (G = 0 kcal/mol) traversing two low-lying transition states (G = 4.2 and 7.6 kcal/mol). The **Fe−Fe′H** species is at the {Fe(NO)}^{8}-Fe′^{III} redox level as the electrons forming the iron-hydride are donated by Fe^{I} of the reduced Fe′.

There are two pathways shown in Figure 2 for addition of the second proton. Although **Fe−Fe′−S^{DN}H** is the dominant species, the next protonation step, either on S of **Fe−Fe′H** or on Fe′ of **Fe−Fe′−S^{DN}H**, produces the same thiol-hydride, **Fe−Fe′H−S^{DN}H**$^{+}$, and both protonations are thermodynamically favored, with ΔpK_a values of 6.6 or 5.3 kcal/mol, respectively. The spatial positioning of the hydride and the proton on **Fe−Fe′H−S^{DN}H**$^{+}$ allows the coupling reaction over a barrier of G = 11.6 kcal/mol. The resulting H_2 σ-complex **Fe−Fe′H$_2$**$^{+}$ then overcomes another barrier at G = 12.0 kcal/mol to dissociate H_2 and to regenerate the catalyst **Fe−Fe′**$^{+}$. This catalyst cycle thus closes with an [ECEC] mechanism. This mechanism uses the thiolate sulfur as a proton relay. One may argue TFA may directly deliver the proton to the hydride of **Fe-FeH′** to accomplish an intermolecular coupling to form **Fe-FeH$_2$**$^{+}$, skipping the intermediate **Fe-FeH-S^{DN}H′**$^{+}$. The relatively high barrier at 16.2 kcal/mol (Figure S43) renders this possibility less likely. In contrast the delivery of proton into the sulfur open site only incurs a negligible barrier (Figure S43).

Alternatively, **Fe−Fe′H−S^{DN}H**$^{+}$ may accept a third electron at a redox potential of −1.27 V, and the highest reaction barrier for H_2 formation dramatically drops to 4.9 kcal/mol. In this case the reduced **Fe−Fe′** is regenerated instead of **Fe−Fe′**$^{+}$ and closes an E[CECE] working catalytic cycle, in which the first reduction event essentially serves as an activation step. According to the calculations, the current enhancement associated with the second reduction event at −1.32 V (calcd; observed at −1.66 V) is considered to be catalytic and productive in either the slow or fast catalytic cycle, as

DOI: 10.1021/jacs.6b06461
J. Am. Chem. Soc. 2016, 138, 12920−12927

subsequent reduction events are all calculated to be less negative than −1.32 V.

The nickel species **Ni−Fe′**$^{+}$ has mechanisms similar to those of **Fe−Fe′**$^{+}$ with a few exceptions, Figure 3. The first reduction of **Ni−Fe′**$^{+}$ is initially localized on the NiN_2S_2 moiety with its four-membered Ni(μ-SR)$_2$Fe′ unit intact as was that of **Fe−Fe′**. However, the four-coordinate nickel lacks the electronic flexibility of Fe(NO) in **Fe−Fe′** and can only accommodate the added electron on nickel's highly destabilized antibonding $d_{x^2-y^2}$ orbital, achieving an oxidation state of Ni^{I}−Fe′^{II} in **Ni−Fe′***. As a result the calculated redox potential rises significantly to −2.00 V (exp. −1.64 V). Following the reduction, one S−Fe′ bond of the Ni(μ-SR)$_2$Fe′ core breaks to open the Ni−S$_2$-Fe′ ring. The electron previously added to the nickel is concomitantly transferred to the unsaturated (16-e^{-}) Fe′ with bond cleavage, bringing the electron counts back to a 16-e^{-} Ni^{II} and a 17-e^{-} Fe^{I}. This arrangement stabilizes the ring-opened species **Ni−Fe′** by 1.0 kcal/mol, accounting for observed irreversibility of the CV event. The experimental IR shift, −157 cm^{-1} (Figure S10), upon the reduction of **Ni−Fe′**$^{+}$, confirms **Fe−Fe′** (calcd shift: −127 cm^{-1}, Table S12) is the reduced product, rather than **Fe−Fe′*** (calcd shift: −43 cm^{-1}).

In the absence of acid, following the ring-opening process and intramolecular charge transfer, the successive reduction on **Ni−Fe′** puts the second electron again within the Ni$^{II/I}$ couple. The calculations also affirm that the first redox potential is more negative than that of any subsequent steps in the catalytic cycles in the presence of TFA (Figure 3), so that the CV current enhancement at −1.64 V is acknowledged as catalytic. The follow-up protonation on **Ni−Fe′** goes directly to the reduced Fe′ rather than S, as the Fe^{I} has sufficient electron density to convert the proton into a Fe^{III}-hydride. The next steps are similar to those of **Fe−Fe′**$^{+}$ in Figure 2. The **Ni−Fe′**$^{+}$ may also have two working catalytic cycles, either [ECEC] or E[CECE] depending on the occurrence of a nonmandatory, third reduction event.

The homoconjugation of TFA,[31,49] i.e., the stabilization of the conjugate base TFA^{-} by another molecule of H-TFA, was evaluated by calculations to enhance the acidity by −5.6 pK_a units (exp. −3.9)[31] on standard conditions. The acidity increase, though less significant when the acid concentration is low, may further facilitate these protonation processes outlined in Figures 2 and 3 at the cost of faster depletion of the available acid on the electrode surface. However, it may not be able to activate another route. An immediate second protonation requires a much stronger acid, *vide supra*.

By proceeding along the predicted mechanistic pathway, the monodentate species, **Ni−Fe″**$^{+}$, breaks its single Fe″−S bond upon reduction, and the complex decomposes, as experimentally observed. The cleaved fragment, the •FeCp(CO)$_2$ radical, is also catalytically active for H_2 production before its fast deactivation by dimerization.[50]

DISCUSSION

This work provides a paradigm for deconvoluting electrocatalytic proton-reduction mechanisms in dithiolate bridged bimetallics. Salient points to be made regarding the mechanistic features of the two [MN_2S_2·CpFe(CO)]$^{+}$ electrocatalysts are as follows:

- The initial electron uptake is at the M in the N_2S_2 pocket, rather than the CpFe′(CO)$^{+}$, for both M = Ni^{II} and {[Fe(NO)}^{7}; the latter however presents a softer, delocalized landing for the electron, without permitting subsequent Fe−H formation, as the iron is not adequately basic (Table S9). Another key difference lies in the fact that the added electron is stored on the {[Fe(NO)}^{8} unit (within the Fe(NO)N_2S_2 metalloligand) throughout the catalytic cycle rendering that unit a "redox-active, spectator ligand"[51] to the reactive center, the CpFe(CO) unit, in the preferred E[CECE] path. In contrast, the first-formed Ni$^{I}N_2S_2$ readily transfers its electron to Fe′, with Ni^{II}-(μ-SR)$_2$-Fe^{I}′ ring opening in advance of protonation. Thus, the Ni^{II} in the monodentate NiN_2S_2 metalloligand cannot accept a proton to form a Ni−H bond resembling the recent NMR characterized Ni-bound hydride in a Ni-R model, which contains a noninnocent ligand with Ni to buffer the electron.[52] Besides, Fe in Fe(NO) is also protected from the proton by open sites on S and on reduced Fe′.
- The hemilability of the MN_2S_2 metalloligand, necessary for producing an open site on the active iron of the CpFe′ unit (a site that is occupied by CO in the **Ni−Fe″**$^{+}$ congener or procatalyst), as well as an available S-base site, is facilitated by reduction of the dithiolate bridged bimetallic. A further role for this hemilability is displayed in the monodentate bridging thiolate bound to the Fe′^{III}-hydride in **Fe−Fe′H−S^{DN}H**$^{+}$. The Fe′^{III} with a formal electron count of 17 is able to accept partial donation from an available π-donor pair on S, serving as a σ + π ligand, while Fe′^{II} in **Fe−Fe′H−S^{DN}H**$^{+}$ is completely saturated, and the S is merely a σ-donating ligand. (See Table S10 for Fe′−S bonding analysis.) This additional π bonding in the oxidized **Fe−Fe′H−S^{DN}H**$^{+}$ species is exemplified by its short Fe′−S bond distance at 2.230 Å that elongates to 2.342 Å upon reduction to the **Fe−Fe′H−S^{DN}H** species.
- The H_2 evolution from the diprotonated, doubly or triply reduced species requires optimally oriented protonated thiol and iron hydride. In this regard it is instructive to compare H^{+}···H^{-} distances in our calculated intermediate thiol-hydrides with experimental data from the doubly protonated P_2N_2FeCpR(CO) complex of Liu et al.,[10] Figure 4, finding concurrence in the reduced **Fe−Fe′H−S^{DN}H** form (1.486 Å) with that is found in the amine pendant base complex (1.489 Å). Note that reduction of **Fe−Fe′H−S^{DN}H**$^{+}$ shortens the H^{+}···H^{-} distance from 2.634 to 1.486 Å via structural shifts in the Fe(NO)N_2S(SH) metalloligand, involving both a rotation around the Fe′−S bond as well as a small change in the τ parameter[53] that defines the extent of square

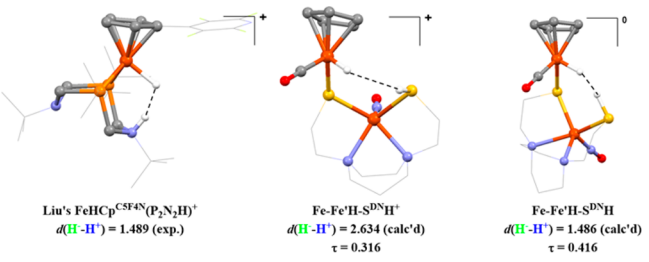

Figure 4. Species featuring proximate proton-hydride pairs and the comparisons of H^{+}−H^{-} distances. The τ value, a measure of square pyramid (τ = 0) vs trigonal bipyramid (τ = 1) geometry in the Fe(NO)N_2S_2 unit.

DOI: 10.1021/jacs.6b06461
J. Am. Chem. Soc. 2016, 138, 12920−12927

pyramid vs trigonal bipyramid character in the Fe(NO)-N_2S(SH) unit. These changes push the proton-hydride pair into a close position, creating an early transition state according to Hammond's postulate,[54] amenable for H_2 elimination via the E[CECE], low barrier path. In contrast at 2.634 Å the H^+/H^- coupling following the [ECEC] mechanistic path must surmount a much higher barrier. Note that the $H^+\cdots H^-$ coupling distance in the Fan and Hall calculated mechanism for proton reduction in the [FeFe]-H_2ase active site is 1.472 Å, remarkably consistent with the experimental value from structure I, and the calculated value (1.486 Å) for our reduced diprotonated intermediate **Fe−Fe′H−S^{DN}H** in Figure 4.[36] Notably, the proton/hydride pair recently characterized in the Ni-R state of the [NiFe]-H_2ase active site is at 2.45 Å,[12] a distance related to the intermediate in our slow route for H_2 production and perhaps consistent with the [NiFe]-H_2ase enzyme's bias toward H_2 uptake and oxidation rather than production.

In conclusion, the well-studied P_2N_2 ligand of Dubois et al.[4] has control of optimal proton placement via the chair/boat interconversion of the six-membered FeP_2C_2N cyclohexane-like ring described in Figure 4,[10] a feature that was exploited in the design and development of further generations of the $Ni(P_2N_2)_2$ catalyst(s) and presaged by nature's azadithiolate bidentate bridging ligand in the [FeFe]-H_2ase active site.[1] The heterobimetallics explored herein demonstrate the possibility for very stable bidentate ligands based on metallodithiolates (a metal-tamed S-donor or nature's version of a phosphine P-donor) that respond to an electrochemical event by switching a coordinate covalent bond into a Lewis acid−base pair and concomitantly placing a proton and hydride within an optimal coupling distance. Easily accessible molecular motions and coordination sphere distortions are available to render the tethered thiolate into a pendant base of greater activity for proton delivery to the metal-hydride. The opportunities for tuning catalysts according to this approach lie both on the metal responsible for the hydride activity and, as we have also shown, the metal that holds and orients the pendant base. Our future plans are to optimize the catalysts via the bidentate S−M−S angle and to pursue experimental evidence for the thiol-hydride pair.

■ ASSOCIATED CONTENT

Supporting Information

The Supporting Information is available free of charge on the ACS Publications website at DOI: 10.1021/jacs.6b06461.

Experimental, additional spectroscopic, electrochemical and computational details (PDF)

X-ray crystallographic data for complexes **Fe−Fe′$^+$**, **Ni−Fe′$^+$**, **Ni−Fe″$^+$** (CIF)

Computational xyz files (ZIP)

■ AUTHOR INFORMATION

Corresponding Authors

*marcetta@chem.tamu.edu

*hall@science.tamu.edu

Present Address

‡School of Chemistry and Chemical Engineering, Henan University of Technology, Zhengzhou 450001, China.

Author Contributions

§These authors contributed equally.

Notes

The authors declare no competing financial interest.

■ ACKNOWLEDGMENTS

We are grateful for financial support from the National Science Foundation (CHE-1266097 to M.Y.D., and CHE-1300787 to M.B.H.), the Robert A. Welch Foundation (A-0924 to M.Y.D. and A-0648 to M.B.H.). Part of the experimental work (salary for Allen Lunsford and Pokhraj Ghosh) was made possible by an NPRP award (NPRP 6-1184-1-224) from the Qatar National Research Fund (a member of Qatar Foundation). The authors acknowledge the Laboratory for Molecular Simulation at Texas A&M University for providing computing resources. Appreciation is expressed to Drs. Eric Wiedner and Aaron Appel for helpful advice dealing with interpretation of the cyclic voltammetry, bulk electrolysis, and gas quantification.

■ REFERENCES

(1) Lubitz, W.; Ogata, H.; Rüdiger, O.; Reijerse, E. *Chem. Rev.* **2014**, *114*, 4081.

(2) Can, M.; Armstrong, F. A.; Ragsdale, S. W. *Chem. Rev.* **2014**, *114*, 4149.

(3) Helm, M. L.; Stewart, M. P.; Bullock, R. M.; DuBois, M. R.; DuBois, D. L. *Science* **2011**, *333*, 863.

(4) DuBois, D. L. *Inorg. Chem.* **2014**, *53*, 3935.

(5) Wilson, A. D.; Shoemaker, R. K.; Miedaner, A.; Muckerman, J. T.; DuBois, D. L.; DuBois, M. R. *Proc. Natl. Acad. Sci. U. S. A.* **2007**, *104*, 6951.

(6) Wilson, A. D.; Newell, R. H.; McNevin, M. J.; Muckerman, J. T.; Rakowski DuBois, M.; DuBois, D. L. *J. Am. Chem. Soc.* **2006**, *128*, 358.

(7) Raugei, S.; Chen, S.; Ho, M.-H.; Ginovska-Pangovska, B.; Rousseau, R. J.; Dupuis, M.; DuBois, D. L.; Bullock, R. M. *Chem. - Eur. J.* **2012**, *18*, 6493.

(8) Stewart, M. P.; Ho, M.-H.; Wiese, S.; Lindstrom, M. L.; Thogerson, C. E.; Raugei, S.; Bullock, R. M.; Helm, M. L. *J. Am. Chem. Soc.* **2013**, *135*, 6033.

(9) Liu, T.; Chen, S.; O'Hagan, M. J.; Rakowski DuBois, M.; Bullock, R. M.; DuBois, D. L. *J. Am. Chem. Soc.* **2012**, *134*, 6257.

(10) Liu, T.; DuBois, D. L.; Bullock, R. M. *Nat. Chem.* **2013**, *5*, 228.

(11) Liu, T.; Wang, X.; Hoffmann, C.; DuBois, D. L.; Bullock, R. M. *Angew. Chem., Int. Ed.* **2014**, *53*, 5300.

(12) Ogata, H.; Nishikawa, K.; Lubitz, W. *Nature* **2015**, *520*, 571.

(13) Dementin, S.; Burlat, B.; De Lacey, A. L.; Pardo, A.; Adryanczyk-Perrier, G.; Guigliarelli, B.; Fernandez, V. M.; Rousset, M. *J. Biol. Chem.* **2004**, *279*, 10508.

(14) Niu, S.; Hall, M. B. *Inorg. Chem.* **2001**, *40*, 6201.

(15) Ogo, S.; Ichikawa, K.; Kishima, T.; Matsumoto, T.; Nakai, H.; Kusaka, K.; Ohhara, T. *Science* **2013**, *339*, 682.

(16) Denny, J. A.; Darensbourg, M. Y. *Chem. Rev.* **2015**, *115*, 5248.

(17) Nguyen, N. T.; Mori, Y.; Matsumoto, T.; Yatabe, T.; Kabe, R.; Nakai, H.; Yoon, K.-S.; Ogo, S. *Chem. Commun.* **2014**, *50*, 13385.

(18) Yang, D.; Li, Y.; Su, L.; Wang, B.; Qu, J. *Eur. J. Inorg. Chem.* **2015**, *2015*, 2965.

(19) Zhu, W.; Marr, A. C.; Wang, Q.; Neese, F.; Spencer, D. J. E.; Blake, A. J.; Cooke, P. A.; Wilson, C.; Schröder, M. *Proc. Natl. Acad. Sci. U. S. A.* **2005**, *102*, 18280.

(20) Canaguier, S.; Field, M.; Oudart, Y.; Pecaut, J.; Fontecave, M.; Artero, V. *Chem. Commun.* **2010**, *46*, 5876.

(21) Weber, K.; Erdem, Ö. F.; Bill, E.; Weyhermüller, T.; Lubitz, W. *Inorg. Chem.* **2014**, *53*, 6329.

(22) Reynolds, M. A.; Rauchfuss, T. B.; Wilson, S. R. *Organometallics* **2003**, *22*, 1619.

(23) Kim, K.; Matsumoto, T.; Robertson, A.; Nakai, H.; Ogo, S. *Chem. - Asian J.* **2012**, *7*, 1394.

DOI: 10.1021/jacs.6b06461
J. Am. Chem. Soc. 2016, 138, 12920−12927

(24) Kishima, T.; Matsumoto, T.; Nakai, H.; Hayami, S.; Ohta, T.; Ogo, S. *Angew. Chem., Int. Ed.* **2016**, *55*, 724.
(25) Kure, B.; Sano, M.; Nakajima, T.; Tanase, T. *Organometallics* **2014**, *33*, 3950.
(26) Kim, K.; Kishima, T.; Matsumoto, T.; Nakai, H.; Ogo, S. *Organometallics* **2013**, *32*, 79.
(27) Chiang, C.-Y.; Miller, M. L.; Reibenspies, J. H.; Darensbourg, M. Y. *J. Am. Chem. Soc.* **2004**, *126*, 10867.
(28) Chiang, C.-Y.; Lee, J.; Dalrymple, C.; Sarahan, M. C.; Reibenspies, J. H.; Darensbourg, M. Y. *Inorg. Chem.* **2005**, *44*, 9007.
(29) Hsieh, C.-H.; Ding, S.; Erdem, O. F.; Crouthers, D. J.; Liu, T.; McCrory, C. C. L.; Lubitz, W.; Popescu, C. V.; Reibenspies, J. H.; Hall, M. B.; Darensbourg, M. Y. *Nat. Commun.* **2014**, *5*, 3684.
(30) Smee, J. J.; Miller, M. L.; Grapperhaus, C. A.; Reibenspies, J. H.; Darensbourg, M. Y. *Inorg. Chem.* **2001**, *40*, 3601.
(31) Fourmond, V.; Jacques, P. A.; Fontecave, M.; Artero, V. *Inorg. Chem.* **2010**, *49*, 10338.
(32) Felton, G. A. N.; Glass, R. S.; Lichtenberger, D. L.; Evans, D. H. *Inorg. Chem.* **2006**, *45*, 9181.
(33) Appel, A. M.; Helm, M. L. *ACS Catal.* **2014**, *4*, 630.
(34) Wiese, S.; Kilgore, U. J.; Ho, M.-H.; Raugei, S.; DuBois, D. L.; Bullock, R. M.; Helm, M. L. *ACS Catal.* **2013**, *3*, 2527.
(35) Smieja, J. M.; Benson, E. E.; Kumar, B.; Grice, K. A.; Seu, C. S.; Miller, A. J. M.; Mayer, J. M.; Kubiak, C. P. *Proc. Natl. Acad. Sci. U. S. A.* **2012**, *109*, 15646.
(36) Cheng, T. Y.; Bullock, R. M. *J. Am. Chem. Soc.* **1999**, *121*, 3150.
(37) Surawatanawong, P.; Tye, J. W.; Darensbourg, M. Y.; Hall, M. B. *Dalton Trans.* **2010**, *39*, 3093.
(38) Siegbahn, P. E. M.; Tye, J. W.; Hall, M. B. *Chem. Rev.* **2007**, *107*, 4414.
(39) Marenich, A. V.; Ho, J.; Coote, M. L.; Cramer, C. J.; Truhlar, D. G. *Phys. Chem. Chem. Phys.* **2014**, *16*, 15068.
(40) Liu, Z.-P.; Hu, P. *J. Am. Chem. Soc.* **2002**, *124*, 5175.
(41) Liu, Z.-P.; Hu, P. *J. Chem. Phys.* **2002**, *117*, 8177.
(42) Fan, H.-J.; Hall, M. B. *J. Am. Chem. Soc.* **2001**, *123*, 3828.
(43) Cao, Z.; Hall, M. B. *J. Am. Chem. Soc.* **2001**, *123*, 3734.
(44) Berggren, G.; Adamska, A.; Lambertz, C.; Simmons, T. R.; Esselborn, J.; Atta, M.; Gambarelli, S.; Mouesca, J. M.; Reijerse, E.; Lubitz, W.; Happe, T.; Artero, V.; Fontecave, M. *Nature* **2013**, *499*, 66.
(45) Esselborn, J.; Lambertz, C.; Adamska-Venkatesh, A.; Simmons, T.; Berggren, G.; Noth, J.; Siebel, J.; Hemschemeier, A.; Artero, V.; Reijerse, E.; Fontecave, M.; Lubitz, W.; Happe, T. *Nat. Chem. Biol.* **2013**, *9*, 607.
(46) Siebel, J. F.; Adamska-Venkatesh, A.; Weber, K.; Rumpel, S.; Reijerse, E.; Lubitz, W. *Biochemistry* **2015**, *54*, 1474.
(47) Esselborn, J.; Muraki, N.; Klein, K.; Engelbrecht, V.; Metzler-Nolte, N.; Apfel, U. P.; Hofmann, E.; Kurisu, G.; Happe, T. *Chem. Sci.* **2016**, *7*, 959.
(48) Sun, N.; Liu, L. V.; Dey, A.; Villar-Acevedo, G.; Kovacs, J. A.; Darensbourg, M. Y.; Hodgson, K. O.; Hedman, B.; Solomon, E. I. *Inorg. Chem.* **2011**, *50*, 427.
(49) Coetzee, J. F.; Padmanabhan, G. R. *J. Am. Chem. Soc.* **1965**, *87*, 5005.
(50) Artero, V.; Fontecave, M. *C. R. Chim.* **2008**, *11*, 926.
(51) Luca, O. R.; Crabtree, R. H. *Chem. Soc. Rev.* **2013**, *42*, 1440.
(52) Brazzolotto, D.; Gennari, M.; Queyriaux, N.; Simmons, T. R.; Pécaut, J.; Demeshko, S.; Meyer, F.; Orio, M.; Artero, V.; Duboc, C. *Nat. Chem.* **2016**, DOI: 10.1038/nchem.2575.
(53) Addison, A. W.; Rao, T. N.; Reedijk, J.; van Rijn, J.; Verschoor, G. C. *J. Chem. Soc., Dalton Trans.* **1984**, 1349.
(54) Hammond, G. S. *J. Am. Chem. Soc.* **1955**, *77*, 334.

DOI: 10.1021/jacs.6b06461
J. Am. Chem. Soc. 2016, 138, 12920−12927